communications earth & environment

ARTICLE

https://doi.org/10.1038/s43247-021-00286-5 OPEN

Networked configurations as an emergent property of transverse aeolian ridges on Mars

T. P. Nagle-McNaughton [1]✉ & L. A. Scuderi[1]

Transverse aeolian ridges – enigmatic Martian features without a proven terrestrial analog – are increasingly important to our understanding of Martian surface processes. However, it is not well understood how the relationships between different ridges evolve. Here we present a hypothesis for the development of complex hexagonal networks from simple linear forms by analyzing HiRISE images from the Mars Reconnaissance Orbiter. We identify variable morphologies which show the presence of secondary ridges, feathered transverse aeolian ridges and both rectangular and hexagonal networks. We propose that the formation of secondary ridges and the reactivation of primary ridge crests produces sinuous networks which then progress from rectangular cells towards eventual hexagonal cells. This morphological progression may be explained by the ridges acting as roughness elements due to their increased spatial density which would drive a transition from two-dimensional bedforms under three-dimensional flow conditions, to three-dimensional bedforms under two-dimensional flow conditions.

[1] Department of Earth and Planetary Science, The University of New Mexico, Northrop Hall, 221 Yale Boulevard Northeast, Albuquerque, NM, USA. ✉email: timnaglemcnaughton@unm.edu

Transverse aeolian ridges (TARs), bright linear bedforms first documented in Mars Orbiter Camera (MOC) data[1–3], are widespread on Mars, however, their distribution and role in the Martian sedimentary system and their relationship to Martian atmospheric conditions is poorly understood[2–7]. Long believed immobile[8–11], recent evidence suggests that TARs may be active over multiyear periods[12]. TARs are morphometrically similar to both ripples and dunes, with symmetric profiles like large wind ripples or small reversing dunes[13,14], and have wavelengths intermediate between ripples and dunes somewhere on the order of 20–100 m[5,12,15–20], TARs are larger than wind ripples on Mars or Earth, but smaller than dunes on either planet[21–26] with amplitudes generally of a few to tens of meters[5,12,15–19] Possible terrestrial proxies include gravel megaripples in Argentina[27,28], megaripples in Iran and Libya[29–31], and reversing dunes in Idaho[32]. Recent work suggests that lower wind pressures on Mars allow megaripples to grow essentially without limit[33]. This hypothesis connects the growth of ripples, megaripples, and TARs into a continuum of forms without the need for alternative formative processes for TARs.

TAR morphotypes are characterized based on crest-line morphology and range from simple with straight and approximately parallel crests without bifurcations to more complex networked closed polygonal forms[1,2,34,35] (Supplementary Table 1, Fig. 1). At least two formative mechanisms have previously been proposed: a dust-deltoid path[6] and barchan-TAR[2] path (Supplementary Fig. 1). Recent work has documented a compound-formation process whereby secondary ridges can form perpendicularly to connect primary ridges[34,35] (Fig. 1a, b). This combination of ridges forms "feathered TARs", a precursor to rectangular-networked TARs (Fig. 1c)[2,34–36]. While the close spatial relationship between feathered TARs and networked TARs has been noted previously, the developmental relationships between these forms have only been addressed recently[34–36]. The connections between sinuous TARs, rectangular networks, and hexagonal networks (Fig. 1d) have been largely unexplored.

We found that primary ridges appear to be reactivated by secondary ridges forming scallops in the primary ridge crest (Fig. 2a–c, Supplementary Fig. 2). These scallops are emergent kink defects in the primary ridge that transform straight crests into sinuous ones, and quadrilateral cells into hexagonal cells. These kinks evolve to form stable-junction angles of ~120°. This process is guided by the evolution of asymmetric stress concentration near vertices, which shifts the vertex; over time, symmetry produces a Y junction[37]. We applied metrics that easily differentiate networked morphologies by (1) the number of vertices per cell and (2) the number of cells per vertex (Fig. 2d, e). Rectangular networked TARs average four vertices per cell and between three and four cells per vertex (Fig. 2d). Hexagonal-networked TARs have six vertices per cell and three cells per vertex (Fig. 2e).

Measures of ridge amplitude further differentiate the forms. Immature rectangular networks have at least two prominent and dissimilar ridge amplitudes: wider and taller primary ridges with narrower and shorter secondary ridges perpendicular to the main ridge crests (Supplementary Figs. 3 and 4). Well-developed

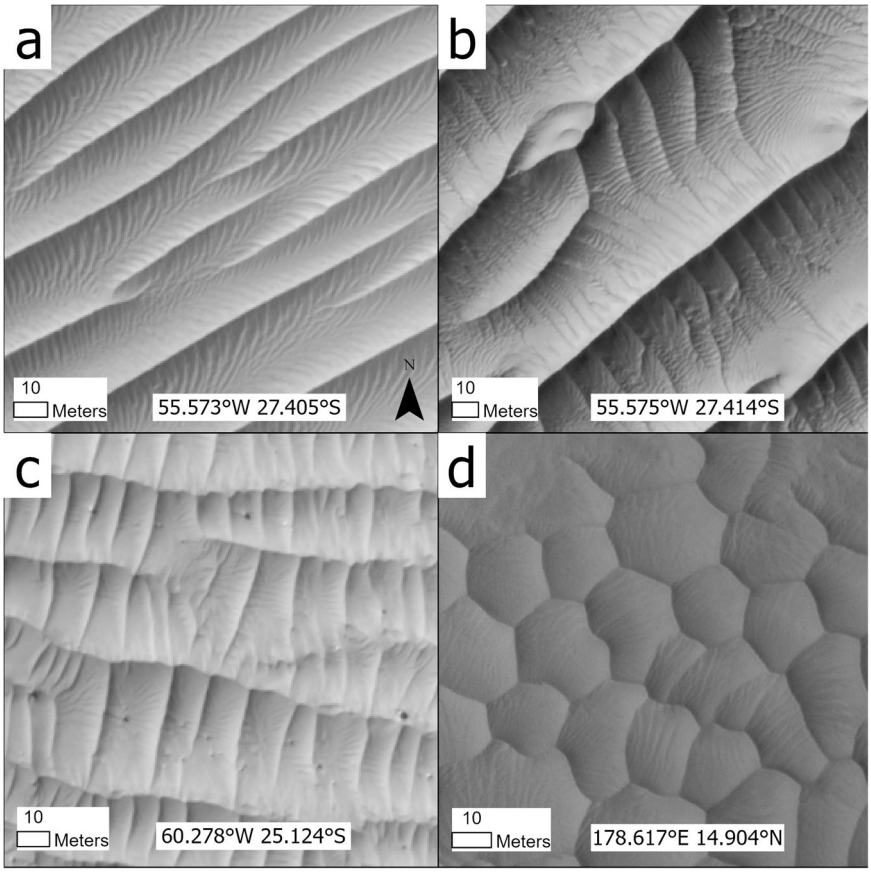


Fig. 1 The progression from simple linear TARs to networked TARs. a Secondary ridges form on larger ridges, producing "feathered" TARs[34,35] (ESP_018597_1525). **b** These secondary ridges become larger and more prominent—often with the formation of tertiary ridge features perpendicular to the secondary crests (ESP_018597_1525). **c** Secondary ridges enlarge and become principal morphological features, forming regular rectangular cells (ESP_017661_1545). **d** Rectangular cells form into a hexagonal network (ESP_064491_1950). Coordinates mark the center of each image. North is up in these and the following images. All HiRISE images credit to NASA/JPL/University of Arizona.

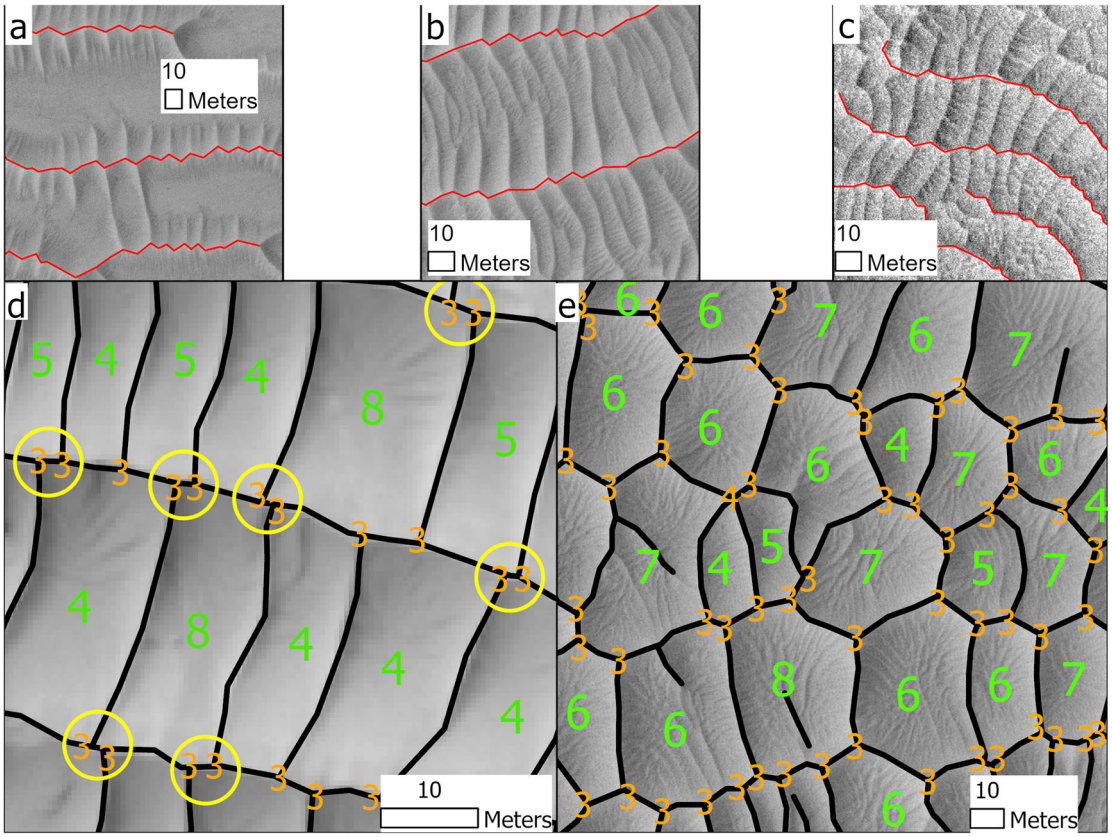


Fig. 2 Scalloping of primary ridges and metrics for differentiating networked morphologies. a–c Note that nearly every kink (annotated in red) in the primary ridges corresponds to the terminus of a secondary ridge, and that the kinks form ~120° angles. Sequence left to right (**a–c**) represents an evolution toward more well-developed secondary ridges (a: ESP_064811_1670; b: ESP_064811_1670; c: ESP_065223_1855). **d–e** Manually traced ridge crests in black, vertices per cell in green, and cells per vertex in orange. **d** Rectangular networked TARs with a median of four vertices per cell, and typically four cells per vertex when the secondary ridges are aligned across primary ridges and three when minor misalignments occur (circled in yellow) (ESP_017661_1545). **e** Hexagonal-networked TARs with a median of six vertices per cell. Hexagonal networked TARs almost exclusively have three cells per vertex (ESP_064877_1670).

rectangular networks exhibit cells that have similar amplitudes, while hexagonal-networked ridges have approximate equal amplitudes in all directions (Supplementary Fig. 4)[34].

Under the hypothesis that hexagonal networks develop from rectangular networks, there is an expectation that a spatial correlation should exist where both forms occur. At these locations (Fig. 3), hexagonal networked TARs display residual rectangular forms (i.e., relict-identifiable primary/secondary ridges) at the margins of the field (Supplementary Fig. 5), whereas the converse pattern—rectangular TARs surrounded by hexagonal TARs—was not observed at any location. Previous studies have noted that TARs have an affinity for topographic depressions[2,3,9,30], and we found that this pattern was especially true for hexagonal-networked TARs (Supplementary Fig. 6, Supplementary Table 2).

Results and discussion

Relating TAR morphologies in a new evolutionary path. Forked TARs represent simple TARs that have developed the defects that would be common in similarly well-developed fields of dunes or ripples. Bifurcation defects are widely accepted to be emergent properties of dune and ripple fields on Earth that develop as the field ages[38–41]. As such, classifying forked TARs as a disparate morphology from simple TARs is an incorrect distinction and one that would not be drawn in a dune or ripple field on Earth.

Feathered TARs are intermediate forms between simple/forked TARs and sinuous or networked TARs[34,35]. Cratering superpositioning shows that the secondary ridges characteristic of feathered TARs usually develop some time after the original crest has been stabilized[34,35], suggesting that feathered TARs form after simple TAR formation. The physics underlying the development of secondary ridges remains poorly understood, but analogous features have been observed in ripples where trailing helical vortices are generated by the main transverse crest[42,43].

Barchan-like TARs form a bent two-pointed shape (Supplementary Fig. 7). They were originally envisioned as a possible precursor morphology from which other TAR forms could be derived[2] (Supplementary Fig. 8). However, well-developed barchan-like TAR features are very rare on Mars, and we argue that a generalized model for TAR development should not be based on a rare edge-case morphology. Rather, we suggest that barchan-like TARs develop from simple transverse forms that experience a combination of unusual windflow conditions and/or sediment supply.

Sinuous TARs were first hypothesized as the product of merging barchan-like TARs[2]. We instead argue that emergent kink defects initiated by secondary ridges on primary ridges create this sinuous morphology (Fig. 4). This conceptualization places the evolution of sinuous TARs after linear simple TARs and before networked TARs.

Rectangular-networked TARs form as secondary ridges grow between nonkinked simple TARs (Fig. 4a–c)[34]. We hypothesize that hexagonal networked TARs develop from sinuous TARs (Fig. 4e–h) or from rectangular TARs that develop kinking (Fig. 4c, d). The

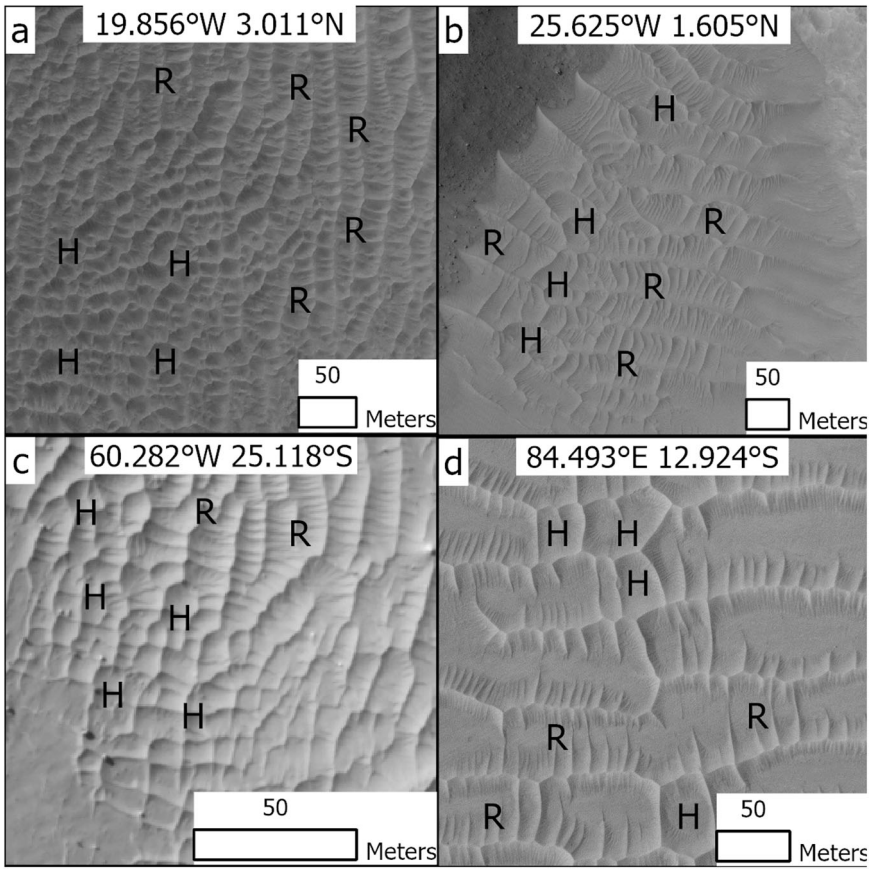


Fig. 3 Spatial relationships between networked TARs. Hexagonal networks (H) are commonly found surrounded by rectangular networks (R) where primary/secondary ridge amplitudes and orientations are still visible (**a** ESP_024266_1830, **b** ESP_027708_1815, **c** ESP_017661_1545, **d** ESP_064811_1670).

original primary/secondary ridges can still be differentiated until the hexagonal network is fully formed (Supplementary Fig. 5). This change from rectangular to hexagonal is supported by the observed spatial patterning outlined above. If rectangular networks evolved from hexagonal forms, we would expect to see primitive hexagonal TARs surrounding well-developed rectangular cells, but the opposite was observed. This correlation is not concrete evidence of this change, but the spatial relationships combined with observations of incomplete kinking are supportive of the pathway outlined here.

Networked TARs as the most-evolved end member. We hypothesize that networked TARs represent the endpoint of TAR evolution. We believe that this evolution is caused by the interaction between the ridges and flow transitioning from a 3D interface to a 2D one (Fig. 5a). Under a 3D-flow regime, the topography of the ridges themselves plays an important role in shaping the flow over the ridges and in generating turbulence that creates subsequent features. Conversely, under a 2D-flow regime, well-connected TARs act as roughness elements in the flow, generating a skimming-flow regime.

Skimming-flow regimes exist when roughness elements are spaced so densely that their wakes completely overlap across the surface, creating stable vortices and causing the flow to pass smoothly above the roughness elements[44–46]. As such, the spatial density and consistent amplitudes of the ridges present in networked TARs make them ideal roughness elements. This notion that bedforms can act as roughness elements themselves is well-established[47,48].

If our evolutionary sequence is correct, there must be some process that forces the system toward networked configurations[41]. Empirical measurements comparing flow over "2D straight dunes"[48,49] (analogous to simple/forked TARs), to 3D forms, suggest such an evolution toward networked forms. This transition proceeds via (1) "Full-width saddle" (barchan TARs), (2) "Full-width lobe" (a reversed barchan form, unobserved in nature), (3) "Sinuous crests" (sinuous TARs), and (4) "Irregular crests"—comparable to hexagonal networked TARs in their plan-view irregularity[49] (Supplementary Fig. 9). Note that these forms are not true dunes, and that they are simply analogous in their crest-line morphologies, this is not to contradict the conceptualization of TARs as megaripples[33].

In these studies, upstream bedforms generated stacked wakes that composed the bulk of the observed turbulent flow[48], consistent with previous predictions[50]. The barchan-like configurations increased boundary shear stress by 38% over the simple/forked 2D forms, the sinuous configuration generated stresses comparable to the simple/forked morphology, and irregular (network-like) configurations generated 20% less stress than the simple/forked form[41]. 3D bedforms reducing flow resistance relative to 2D forms are consistent with previous work conducted over mobile beds[51]. Other studies found that both turbulence intensity and Reynolds stress declined as 3D bedforms developed, with 2D forms naturally evolving toward 3D forms and reaching a stable configuration[51]. This tendency toward 3D forms could explain why TARs change from one morphology to another.

Further, 2D dune forms (analogous to simple TARs) have been documented spontaneously developing into 3D forms (sinuous and networked TARs; see Figure 9 of the study[47]). Other work has observed the development of perpendicular ridges on transverse ridges (termed "bedform spurs"[42,43], similar to secondary ridges documented on TARs[34,35]) created by vortices shed by the primary transverse ridge[28,29].

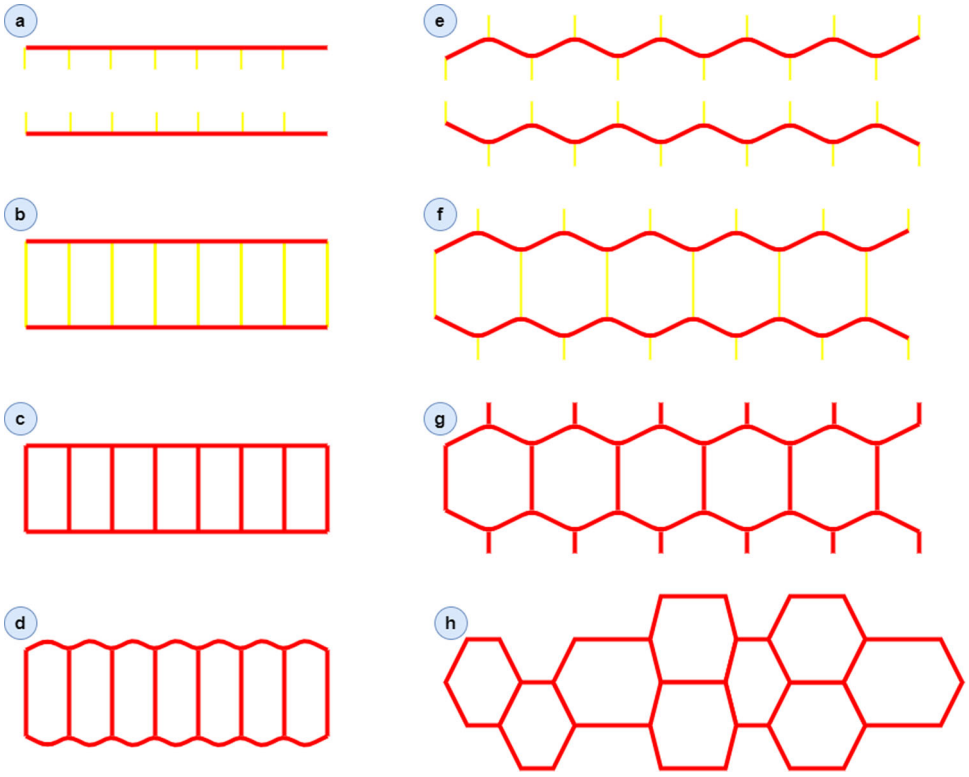


Fig. 4 Sinuous and networked TAR development. Secondary TARs (yellow lines) grow on the main crest (red). Regular growth proceeds from a to b. Reactivation of the primary ridge forms kinked sinuous primary ridges, directly from a to e. Rectangular networked TARs are formed by the growth of secondary ridges between primary ridges that do not experience kinking (**a**–**c**). Hexagonal-networked TARs can develop from rectangular networks that develop kinking (**c**, **d**) or from sinuous TARs (**e**–**g**). In this conceptualization, **d** and **g** are essentially equivalent forms with disparate origins. Over time, the hexagonal networks become more irregular (**h**) and the original primary/secondary ridge structure is lost.

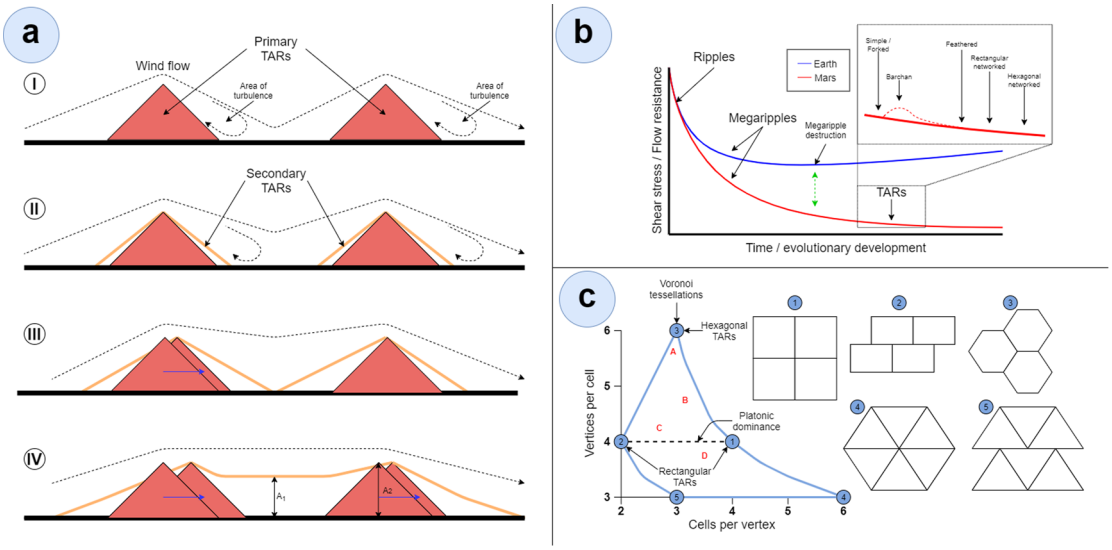


Fig. 5 Conceptual models of TAR development. a Profile view of TARs transitioning from 3D flow to 2D flow. See text for a detailed description. **b** Conceptual model of TAR development on Mars (red line) compared with Earth (blue line). The dashed green arrow marks the point where megaripples on Earth are flattened as they increase in height[33,57,58]. The inset illustrates morphological evolution. **c** All possible convex tiling combinations (surrounded in blue). Natural phenomena in red: (A) basalt fracturing, (B) permafrost, (C) mud cracks, and (D) surface fractures in granite. After Domokos et al. (2020).

Interpretation of the above findings suggests that (1) the scarcity of barchan-like TARs may be the result of barchan configurations generating higher shear stresses, making them more susceptible to activation/reactivation by wind, more transient, and less likely to be stabilized and preserved than other TAR morphologies; (2) more complex TAR morphologies are lower-energy configurations than simple crests, supporting our contention that simple TAR morphologies must be

precursors to composite ones: the system should transition from higher to lower shear stress.

Further research using computational fluid-dynamic simulations of TARs is warranted. Such simulations could measure the shear stresses on fully accurate TAR configurations, including the rectangular and hexagonal network forms that have only been roughly approximated in the current literature. Such a quantitative study could explicitly connect the hypothesized TAR development pathway and the forcing mechanism outlined here. Further, a global survey of TAR morphologies and distributions could provide insight into the developmental relationships between TAR morphologies. There has been some work to automate the mapping of TARs in general using neural networks[52], but there must first be a consensus around the characteristics of each specific morphology as this study attempts to clarify.

If a global database of TAR locations and morphologies were created, it would enable scientists to examine both correlations between local contexts and TARs, such as between the surrounding terrain age or elevation and the predominant TAR morphology. A TAR database could also help characterize the overall abundance of each TAR morphology. Assuming the hypothesized pathway in this paper is correct, the abundance of each TAR morphology could thus be used as a demographic profile of relative TAR development. For example, if a plurality of TARs on Mars were simple, it would suggest that a combination of (1) TARs being relatively young and have not having had time to develop into more complex morphologies, and (2) the conditions required for further TAR development being rare.

Minimum-energy states. Figure 5a illustrates the hypothesized transition from 3D to 2D flow. In (I), two simple TARs (red) form in a flow (dashed line) generating downstream turbulence. In (II), secondary ridges (orange) begin to fill the interridge area, reducing turbulence. In (III), secondary ridges extend crest-to-crest between the primary ridges. Scalloping shifts the primary ridge laterally (blue arrow). Finally, in (IV), the networked configuration interridge amplitude (A_1) is nearly equal to the original primary ridge amplitude (A_2). The flow skims over the networked TARs without much interaction and shear stress and turbulence are minimized.

Figure 5b illustrates a conceptual model of TAR development on Mars (red line) compared with Earth (blue line). The dashed green arrow marks the point where megaripples on Earth are flattened as they increase in height[27,49,50]. On Mars, megaripples are more stable and can grow larger since the lower wind pressures do not impose such a finite limit[27]. The Fig. 5b inset illustrates TAR morphological evolution. Simple/forked TARs develop first; occasionally unstable barchan types form; feathers form on simple TARs and develop into rectangular networks; some rectangular networks finally form hexagonal networks. Figure 5c shows all possible convex tiling combinations. Note the separation of hexagonal patterning (3) from rectangular forms (1, 2). For comparison, natural fracturing phenomena are indicted in red. Of these, basalt fracturing (A) and to a lesser degree, permafrost (B) show similarities to hexagonal TAR forms. Mud cracks (C) and surface fractures in granite (D), while exhibiting space-filling tessellations, are more similar to rectangular TAR networks.

Similarities between TAR geometries and patterns of tiling and fragmentation[44] span a spectrum between "Platonic" quadrangles[53] (those tiling patterns with four vertices per cell) and Voronoi hexagons[54] (a mathematical method for partitioning space) that mirrors the rectangle/hexagon patterning observed in networked TARs (Fig. 5c). The visual similarity between networked TARs and Voronoi tessellations[55,56] is striking (Supplementary Fig. 10).

Our results suggest a connection between fragmentation dimensionality and the flow dimensionality observed with TARs. Quadrangle patterning dominates in 3D fragments, while hexagonal patterning dominates 2D fracturing[53]. We observe that 3D fragments share patterning with TARs in 3D flow (six vertices per cell, three cells per vertex), and 2D fragments share patterning with TARs in 2D flow (four vertices per cell, 3–4 cells per vertex). The connection between these concepts is abstract, likely in the evolution of both systems toward lower-energy configurations and in the efficient partitioning of space (e.g., during the cooling of basalt or the evaporation of water from mud). While at the moment speculative, we feel that this could be a fruitful avenue for future theoretical geomorphic research.

Methods

HiRISE images were downloaded as map-projected JPEG2000 files using the 'random image' tool on www.uahirise.org. Images containing examples of well-developed networked TARs or other relevant features were integrated into an ArcGIS Pro 2.7.2 file[59]. If an image contained large scan-line artifacts, earlier or later images of the same area were downloaded to mitigate errors from these artifacts. If interesting TARs were near the edge of an image or were cut off in the original images, adjacent images were searched for and downloaded where available. The distribution of the selected images can be seen in Supplementary Fig. 11, and a complete list of images used is found in Supplementary Table 3.

Ridge crests were manually traced using polylines in a geodatabase. Where DTMs were available, amplitude transects were derived via the 'interpolate shape' tool in ArcGIS Pro (pro.arcgis.com/en/pro-app/latest/tool-reference/3d-analyst/interpolate-shape.htm). Where DTMs were not available but stereoimage pairs were, visual estimations were made using the full-resolution anaglyphs. Examples of primary ridge reactivation by secondary ridge scalloping were traced and saved as a line file in the geodatabase. Hanging-ridge segments were excluded from our networked TAR metrics: for "cells per vertex", only completely closed polygons were included and for "number of vertices per cell", only vertices that were part of a completely closed polygon were included.

The Voronoi diagram in Supplementary Fig. 10 was generated by the Create Theissan Polygons tool in ArcGIS Pro (pro.arcgis.com/en/pro-app/latest/tool-reference/analysis/create-thiessen-polygons.htm). The centroid points of the manually traced cells were extracted via geometry calculation, and subsequently given as input to create the synthetic cells.

Data availability

All HiRISE images analyzed in this study are publicly available from NASA/JPL/University of Arizona: https://www.uahirise.org/.

Received: 1 July 2021; Accepted: 17 September 2021;
Published online: 13 October 2021

References

1. Wilson, S. A. & Zimbelman, J. R. Latitude-dependent nature and physical characteristics of transverse aeolian ridges on Mars. *J. Geophys. Res. E Planets* **109**, 1–12 (2004).
2. Balme, M., Berman, D. C., Bourke, M. C. & Zimbelman, J. R. Transverse aeolian ridges (TARs) on Mars. *Geomorphology* **101**, 703–720 (2008).
3. Berman, D. C., Balme, M. R., Rafkin, S. C. R. & Zimbelman, J. R. Transverse aeolian ridges (TARs) on Mars II: distributions, orientations, and ages. *Icarus* **213**, 116–130 (2011).
4. Chojnacki, M., Hargitai, H. & Kereszturi, Á. *Encyclopedia of Planetary Landforms*, https://doi.org/10.1007/978-1-4614-9213-9 (Springer, 2015).
5. Geissler, P. E. & Wilgus, J. T. The morphology of transverse aeolian ridges on Mars. *Aeolian Res.* **26**, 63–71 (2017).
6. Geissler, P. E. The birth and death of transverse aeolian ridges on mars. *J. Geophys. Res. Planets*, https://doi.org/10.1002/2014JE004633 (2014).
7. Bridges, N. T. et al. Planet-wide sand motion on mars. *Geology* **40**, 31–34 (2012).
8. Fenton, L. K., Bandfield, J. L. & Ward, A. W. Aeolian processes in proctor crater on mars: sedimentary history as analyzed from multiple data sets. *J. Geophys. Res. E Planets* **108**, 3–1 (2003).
9. Bridges, N., Geissler, P., Silvestro, S. & Banks, M. Bedform migration on mars: current results and future plans. *Aeolian Res.* **9**, 133–151 (2013).
10. Berman, D. C., Balme, M. R., Michalski, J. R., Clark, S. C. & Joseph, E. C. S. High-resolution investigations of transverse aeolian ridges on Mars. *Icarus* **312**, 247–266 (2018).

11. Reiss, D., van Gasselt, S., Neukum, G. & Jaumann, R. Absolute dune ages and implications for the time of formation of gullies in Nirgal Vallis, Mars. *J. Geophys. Res. E Planets* **109**, 1–9 (2004).
12. Silvestro, S. et al. Megaripple Migration on Mars. *J. Geophys. Res. Planets*, https://doi.org/10.1029/2020je006446 (2020).
13. Zimbelman, J. R. & Williams, S. H. Dunes versus ripples: topographic profiling across terrestrial examples, with application to the interpretation offeatures on Mars. In *AGU 88 Abstract P34A-07* (2007).
14. Shockey, K. M. & Zimbelman, J. R. Analysis of transverse aeolian ridge profiles derived from HiRISE images of Mars. *Earth Surf. Processes Landf.* **38**, 179–182 (2013).
15. Sullivan, R. et al. Wind-driven particle mobility on Mars: insights from mars exploration Rover observations at "El Dorado" and surroundings at Gusev Crater. *J. Geophys. Res.* **113**, 1–70 (2008).
16. Silvestro, S., Fenton, L. K., Vaz, D. A., Bridges, N. T. & Ori, G. G. Ripple migration and dune activity on Mars: Evidence for dynamic wind processes. *Geophys. Res. Lett.* **37**, 5–10 (2010).
17. Fenton, L. K., Silvestro, S. & Kocurek, G. Transverse aeolian ridge growth mechanisms and pattern evolution in Scandia Cavi. *Mars Front. Earth Sci.* **8**, 1–17 (2021).
18. Zimbelman, J. R. Decameter-scale ripple-like features in Nirgal Vallis as revealed in THEMIS and MOC imaging data. In *Sixth International Conference on Mars* July 20–25 2003, Pasadena, California, abstract no.3028 (2003).
19. Chojnacki, M., Banks, M. E., Fenton, L. K. & Urso, A. C. Boundary condition controls on the high-sand-flux regions of Mars. *Geology* **47**, 427–430 (2019).
20. Hugenholtz, C. H., Barchyn, T. E. & Boulding, A. Morphology of transverse aeolian ridges (TARs) on Mars from a large sample: further evidence of a megaripple origin? *Icarus* **286**, 193–201 (2017).
21. Bourke, M. C., Balme, M., Beyer, R. A., Williams, K. K. & Zimbelman, J. A comparison of methods used to estimate the height of sand dunes on Mars. *Geomorphology* **81**, 440–452 (2006).
22. Wilson, S., Zimbelman, J. R. & Williams, S. H. Large aeolian ripples: extrapolations from earth to mars. in *Lunar and Planetary Science Conference*. 1–2 (2003).
23. Williams, S. H., Zimbelman, J. R. & Ward, A. W. Large Ripples on Earth and Mars. In *33rd Annual Lunar and Planetary Science Conference*, March 11–15, 2002, Houston, Texas, abstract no.1508 (2002).
24. Milana, J. P. Largest wind ripples on earth? *Geology* **37**, 343–346 (2009).
25. Leeder, M. R. *Sedimentology: Process and Product* (Springer Science & Business Media, 1982).
26. Lapotre, M. G. A. et al. Large wind ripples on mars: a record of atmospheric evolution. *Science* **353**, 55–58 (2016).
27. Hugenholtz, C. H., Barchyn, T. E. & Favaro, E. A. Formation of periodic bedrock ridges on earth. *Aeolian Res.* **18**, 135–144 (2015).
28. de Silva, S. L., Spagnuolo, M. G., Bridges, N. T. & Zimbelman, J. R. Gravel-mantled megaripples of the Argentinean Puna: a model for their origin and growth with implications for mars. *Bull. Geol. Soc. Am.* **125**, 1912–1929 (2013).
29. Foroutan, M. & Zimbelman, J. R. Mega-ripples in Iran: a new analog for transverse aeolian ridges on mars. *Icarus* **274**, 99–105 (2016).
30. Foroutan, M., Steinmetz, G., Zimbelman, J. R. & Duguay, C. R. Megaripples at Wau-an-Namus, Libya: a new analog for similar features on mars. *Icarus* **319**, 840–851 (2019).
31. Hugenholtz, C. H. & Barchyn, T. E. A terrestrial analog for transverse aeolian ridges (TARs): environment, morphometry, and recent dynamics. *Icarus* **289**, 239–253 (2017).
32. Zimbelman, J. R. & Scheidt, S. P. Precision topography of a reversing sand dune at Bruneau Dunes, Idaho, as an analog for transverse aeolian ridges on mars. *Icarus* **230**, 29–37 (2014).
33. Sullivan, R., Kok, J. F., Katra, I. & Yizhaq, H. A broad continuum of aeolian impact ripple morphologies on mars is enabled by low wind dynamic pressures. *J. Geophys. Res. Planets* **125**, 1–39 (2020).
34. Nagle-McNaughton, T. P. & Scuderi, L. A. A geomorphological case for multistage evolution of transverse aeolian ridges. *Planet. Space Sci.* **200**, 105192 (2021).
35. Nagle-McNaughton, T. P. & Scuderi, L. A. Multistage evolution in transverse aeolian ridges. *Remote Sens.* **13**, 1329 (2021).
36. Bhardwaj, A., Sam, L., Martin-Torres, F. J. & Zorzano, M.-P. Distribution and morphologies of transverse aeolian ridges in ExoMars 2020 rover landing site. *Remote Sens.* **11**, 912 (2019).
37. Goehring, L. Evolving fracture patterns: columnar joints, mud cracks and polygonal terrain. *Philos. Trans. Royal Soc. A Math. Phys. Eng. Sci.* **371**, 20120353 (2013).
38. Werner, B. T. & Kocurek, G. Bed-form dynamics: does the tail wag the dog? *Geology* **25**, 771–774 (1997).
39. Werner, B. T. & Kocurek, G. Bedform spacing from defect dynamics. *Geology* **27**, 727–730 (1999).
40. Anderson, R. S. Eolian ripples as examples of self-organization in geomorphological systems. *Earth Sci. Rev.* **29**, 77–96 (1990).
41. Kocurek, G., Ewing, R. C. & Mohrig, D. How do bedform patterns arise? New views on the role of bedform interactions within a set of boundary conditions. *Earth Surf. Process. Landf.* **35**, 51–63 (2010).
42. Swanson, T., Mohrig, D., Kocurek, G., Perillo, M. & Venditti, J. Bedform spurs: a result of a trailing helical vortex wake. *Sedimentology* **65**, 191–208 (2018).
43. Mason, J. et al. Pattern evolution and interactions in subaqueous dune fields: North Loup River, Nebraska, USA. *J. Sediment. Res.* **90**, 1734–1746 (2020).
44. Lee, B. E. & Soliman, B. F. An investigation of the forces on three dimensional bluff bodies in lough wall turbulent boundary layers. *J. Fluids Eng.* **99**, 503–509 (1977).
45. Raupach, M. R. Drag and drag partition on rough surfaces. *Boundary-Layer Meteorol.* **60**, 375–395 (1992).
46. Raupach, M. R., Gillette, D. A. & Leys, J. F. The effect of roughness elements on wind erosion threshold. *J. Geophys. Res. Atmos.* **98**, 3023–3029 (1993).
47. Venditti, J. G., Church, M. & Bennett, S. J. On the transition between 2D and 3D dunes. *Sedimentology* **52**, 1343–1359 (2005).
48. Venditti, J. G. Turbulent flow and drag over fixed two- and three-dimensional dunes. *J. Geophys. Res. Earth Surf.*, 10.1029/2006JF000650 (2007).
49. Rubin, D. M. A unifying model for planform straightness of ripples and dunes in air and water. *Earth Sci. Rev.* **113**, 176–185 (2012).
50. Nelson, J. M. & Smith, J. D. Mechanics of flow over ripples and dunes. *J. Geophys. Res.* **94**, 8146–8162 (1989).
51. Schindler, R. J. & Robert, A. Flow and turbulence structure across the ripple-dune transition: an experiment under mobile bed conditions. *Sedimentology* **52**, 627–649 (2005).
52. Nagle-Mcnaughton, T., McClanahan, T. & Scuderi, L. PlaNet: a neural network for detecting transverse aeolian ridges on mars. *Remote Sens.* **12**, 1–15 (2020).
53. Domokos, G., Jerolmack, D. J., Kun, F. & Ke, J. T. R. Plato's cube and the natural geometry of fragmentation. *Proc. Natl. Acad. Sci. USA.* **117**, 18178–18185 (2020).
54. Jerauld, G. R., Scriven, L. E. & Davis, H. T. Percolation and conduction on the 3D Voronoi and regular networks: a second case study in topological disorder. *J. Phys. C Solid State Phys.* **17**, 3429–3439 (1984).
55. Erwig, M. The graph Voronoi diagram with applications. *Networks* **36**, 156–163 (2000).
56. Du, Q., Faber, V. & Gunzburger, M. Centroidal Voronoi tessellations: applications and algorithms. *SIAM Rev.* **41**, 637–676 (1999).
57. Yizhaq, H., Katra, I., Kok, J. F. & Isenberg, O. Transverse instability of megaripples. *Geology* **40**, 459–462 (2012).
58. Yizhaq, H. et al. The origin of the transverse instability of aeolian megaripples. *Earth Planet. Sci. Lett.* **512**, 59–70 (2019).
59. ESRI. ArcGIS Pro 2.7. *Environmental Systems Research Institute ArcGIS desktop* (2020).

Acknowledgements

The authors thank the peer reviewers for their time and help in improving this paper. The authors would like to thank Joshua Sokol for his excellent science writing that brought geometric tiling to the first author's attention. This project was supported by NASA Doctoral Fellowship 80NSSC19K1676.

Author contributions

T.N.-McNaughton: Conceptualization, methodology, software, formal analysis, investigation, data curation, writing–original draft, writing–review and editing, visualization, and funding acquisition. L.S.: Conceptualization, methodology, resources, formal analysis, investigation, writing-review and editing, project administration, and funding acquisition.

Competing interests

The authors declare no competing interests.

Additional information

Supplementary information The online version contains supplementary material available at https://doi.org/10.1038/s43247-021-00286-5.

Correspondence and requests for materials should be addressed to T. P. Nagle-McNaughton.

Peer review information *Communications Earth & Environment Materials* thanks James Zimbelman and Hezi Yizhaq for their contribution to the peer review of this work. Primary Handling Editor: Joe Aslin.

Reprints and permission information is available at http://www.nature.com/reprints

Publisher's note Springer Nature remains neutral with regard to jurisdictional claims in published maps and institutional affiliations.



Open Access This article is licensed under a Creative Commons Attribution 4.0 International License, which permits use, sharing, adaptation, distribution and reproduction in any medium or format, as long as you give appropriate credit to the original author(s) and the source, provide a link to the Creative Commons license, and indicate if changes were made. The images or other third party material in this article are included in the article's Creative Commons license, unless indicated otherwise in a credit line to the material. If material is not included in the article's Creative Commons license and your intended use is not permitted by statutory regulation or exceeds the permitted use, you will need to obtain permission directly from the copyright holder. To view a copy of this license, visit http://creativecommons.org/licenses/by/4.0/.

This is a U.S. government work and not under copyright protection in the U.S.; foreign copyright protection may apply 2021